Electronic
Research Archive

https://www.aimspress.com/journal/era

ERA, 33(10): 6322–6342.
DOI: 10.3934/era.2025279
Received: 24 July 2025
Revised: 12 October 2025
Accepted: 15 October 2025
Published: 27 October 2025

Research article

Physics-informed neural network-based finishing entry temperature correction: A hybrid mechanistic and data-driven approach

Shengyue Zong[1], **Zhao Yang**[2] **and Jinyan Li**[3,*]

[1] National Engineering Research Center for Advanced Rolling Technology and Intelligent Manufacturing, University of Science and Technology Beijing, Beijing 100083, China

[2] School of Automation and Electrical Engineering, University of Science and Technology Beijing, Beijing 100083, China

[3] Nanjing Steel Group Co., LTD, Nanjing 210035, China

* **Correspondence:** Email: lijinyan@njsteel.com.cn.

Abstract: In the hot-rolled strip steel production process, the finishing entry temperature (FET) is directly related to the mechanical properties, microstructural uniformity, and surface quality of the steel, while also having a significant impact on energy consumption and carbon emissions. Traditional temperature measurement and prediction methods each have their limitations, such as large measurement errors, high computational complexity, or overfitting issues. To address these challenges, this paper proposes a finishing entry temperature-physics-informed neural network (FET-PINN) method that integrates rough delivery temperature (RDT) data with thermodynamic equations. First, by leveraging the advantage that the temperature in the RDT region more closely approximates the true billet temperature, an initial prediction of the FET was obtained via a FET-PINN model in conjunction with thermodynamic equations. Subsequently, to account for model errors, the fusion weight was calculated using a nonlinear least squares method, and a weighted averaging approach was employed to fuse this predicted value with the temperature computed from instrumentation measurements, thereby achieving a more accurate temperature estimation. Finally, considering the effect of FET on the subsequent rolling force, the paper evaluated the model comprehensively by comparing the predicted rolling force with the actual rolling force using the coefficient of determination (R^2), root mean square error (RMSE), mean absolute error (MAE), and mean absolute percentage error (MAPE) as evaluation metrics. Experimental results demonstrated that the proposed method enhances the accuracy of temperature prediction and provides effective technical support for temperature control in hot rolling processes.

Keywords: nonlinear least squares method; physics-informed neural network; temperature prediction; temperature fusion

1. Introduction

In the hot-rolled strip steel production process, the finishing entry temperature (FET)—i.e., the temperature at the mill entry—is a critical parameter affecting product quality and energy consumption. Precise control of FET is essential for ensuring the mechanical properties, microstructural uniformity, and surface quality of the final product. Accurate prediction of FET not only helps optimize rolling process parameters but also reduces product defects caused by temperature deviations, lowers energy consumption, and improves production efficiency. In actual production, FET is influenced by multiple factors, including the furnace discharge temperature, intermediate cooling process, heat transfer in the hot rolling line, and ambient temperature. Therefore, developing high-precision prediction models is of significant importance [1–3].

Current research methods for temperature prediction include temperature monitoring based on measurement instruments, calculations based on physical models, and predictions based on data-driven models. For example, Bo et al. [4] proposed a segmented modeling strategy based on industrial big data to predict the FET of continuous hot rolling using data-driven methods such as random forest and a support vector machine. In [5], a deep belief network (DBN) was employed for FET prediction by combining an unsupervised pretraining phase with a fine-tuning strategy. In [6], a multi-physical field coupled method for predicting the rolling process temperature was presented based on finite element simulation and experimental data. In [7], a deep learning model integrating long short-term memory (LSTM) and attention mechanisms was developed to predict the temperature control time for wide-thick plate rolling production, thereby indirectly improving the stability of the FET. In [8], a dynamic correction method based on the heat transfer equation was proposed, along with the development of a steel ladle and intermediate ladle molten steel temperature prediction model, to optimize temperature control in the continuous casting and rolling process. In [9], a method that combined fuzzy C-means clustering with fuzzy logic was adopted to perform cluster analysis on historical process data, and a fuzzy inference system was utilized to predict the FET. In [10], an improved Wagner-Hagras OLS-BP hybrid algorithm was introduced to train an interval type-3 non-single-valued fuzzy logic system (IT3 NSFLS-1) for predicting the temperature distribution in the hot-rolled strip steel process. In [11], the performance of neural networks (NN), fuzzy logic systems (FLS), and grey-box models in predicting FET was compared, offering a solution that combines physical consistency with data-driven capability. Sun et al. [12] proposed a physics-informed neural network (PINN) model that embeds thermophysical equations into the neural network to predict the temperature inside the reheating furnace. Zhang et al. [13] introduced a hierarchical feature fusion method, enabling co-prediction of the coiling temperature at both the strip level and the coil level. Yang et al. [14] pioneered the application of graph neural networks (GNNs) to temperature field prediction in reheating furnaces, modeling the spatial correlations of heat transfer between steel slabs.

Although the aforementioned methods can predict FET, they still exhibit significant errors. FET measurement instruments typically detect infrared radiation from the strip surface; however, factors such as oxide scale formation, water vapor interference, and the temperature difference between the surface and core introduce considerable measurement errors. Physical models are computationally complex and difficult to implement in real time, while data-driven models, though capable of capturing the relationship between inputs and temperature, rely on large amounts of historical data, are prone to overfitting, and lack physical interpretability.

By contrast, the measurement of the rough delivery temperature (RDT) is more accurate because the temperature difference between the surface and the interior of the steel in this region is minimal, providing reliable data support for predicting the FET. Compared with other neural network-based prediction methods, the PINN demonstrates significant advantages in terms of computational efficiency and accuracy. By embedding physical equations as constraints within the model, it not only reduces the reliance of purely data-driven approaches on large amounts of training data but also avoids the high computational costs associated with traditional numerical methods. Furthermore, the incorporation of physical laws significantly enhances the model's generalization capability in data-sparse regions, ensuring that the prediction results are both consistent with physical principles and highly accurate. A PINN, which incorporates both physical equations and deep learning, not only ensures that the prediction results abide by physical laws, but also improves computational efficiency, overcomes the limitations of purely data-driven models, and simplifies the physical modeling process [15–18]. Figueredo et al. [19] introduced a hybrid model that combines a PINN and LSTM to accurately predict the dynamic variation of river temperatures. Liao et al. [20] developed a hybrid thermal model that employs a PINN to simultaneously achieve temperature field prediction during the additive manufacturing process. Han et al. [21] integrated a PINN with the Kolmogorov-Arnold network (KAN) method to predict the temperature distribution of composite materials under extreme heat flux in a simulated nuclear environment. Peng et al. [22] proposed a PINN model combined with transfer learning to predict the 3D temperature field in the laser-directed energy deposition (L-DED) process using a single 2D temperature image.

Based on these considerations, this paper proposes a method that combines the RDT T_r and thermodynamic equations within a FET-PINN framework to obtain an initial prediction of the FET, denoted as $\hat{T}_p$. This prediction is then fused with the temperature calculated by the FET measurement instrument, denoted by T_t, to yield the final fused FET $\hat{T}_f$. This approach offers a novel perspective and methodology for precise temperature control in steel production processes. Moreover, since the FET has a significant impact on subsequent finishing rolling force, this paper evaluates the models predictive performance and accuracy by comparing the predicted rolling force $\hat{F}_p$ with the actual rolling force F_f, using the coefficient of determination (R^2), root mean square error (RMSE), mean absolute error (MAE), and mean absolute percentage error (MAPE) as evaluation indices.

The structure of the remainder of the paper is as follows. Section 2 presents the problem description. Section 3 outlines the overall approach. Section 4 establishes the FET-PINN model for predicting the FET based on the RDT. Section 5 describes the fusion estimation of the FET. Section 6 details the algorithm implementation. Section 7 validates the proposed approach through experiments, and Section 8 concludes the paper with future outlooks.

2. Problem description

The scenario investigated in this study is illustrated in Figure 1, focusing on the temperature prediction problem of strip steel as it moves from the roughing mill exit through descaling and other processes to the finishing mill entry. First, by comprehensively utilizing the RDT (denoted as T_r in the figure) and the thermodynamic equations (including the air-cooling heat dissipation processes indicated by ① and ②, and the water-cooling process indicated by ③), the physical model loss term and the boundary condition loss term are constructed. Based on these, a preliminary prediction of the finishing rolling entry temperature $\hat{T}_p$ is obtained using the FET-PINN model. However, due to uncertainties in the model training process and input parameters, predictions relying solely on physical constraints may still exhibit deviations.

To further improve prediction accuracy, this study introduces a weighted fusion method to integrate $\hat{T}_p$ with the measured temperature T_t obtained from the finishing rolling entry temperature sensor. The fusion process is expressed as follows:

$$\hat{T}_f = w_p \hat{T}_p + (1 - w_p) T_t$$

where w_p represents the weight of the FET-PINN-predicted result. To ensure the optimal fusion effect, the weight w_p is determined using the nonlinear least squares method combined with Newton's iterative algorithm. The final fused temperature $\hat{T}_f$ not only preserves the real-time measurement advantage of the sensor but also effectively mitigates the uncertainty of model-only predictions, thereby achieving a more accurate estimation of the finishing rolling entry temperature.

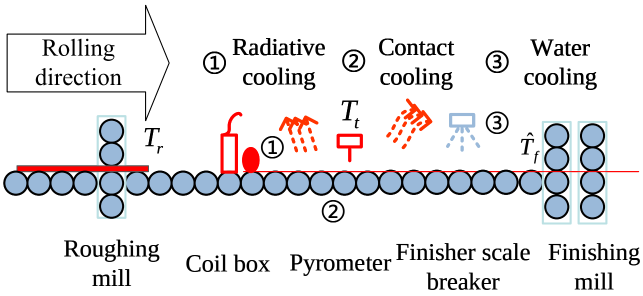

Figure 1. Process site flow chart.

3. Framework

For the calculation of the FET, significant measurement errors exist, causing the measured values to fail to accurately reflect the overall temperature. By contrast, the temperature measurement at the rough rolling exit is more accurate because the RDT location is situated a few meters behind the roughing mill, at which point the temperature difference between the surface and the interior of the steel is minimal and the formation of iron oxide scale is absent. This provides more reliable data support for predicting the FET.

Traditional methods for predicting the FET mainly include physics-based models and data-driven models. Physics-based models can simulate temperature variations based on physical processes such as heat conduction and thermal radiation, and thereby accurately capture the temperature change. However, these methods typically involve heavy computations and complex modeling, and are difficult to apply in real time. On the other hand, data-driven models rely on large volumes of historical data for training and can capture the relationship between inputs and temperature outputs to a certain extent, but they may suffer from overfitting, underfitting, or a lack of interpretability when it comes to explaining complex physical mechanisms.

Based on the above considerations, this paper proposes a prediction method that combines the RDT with thermodynamic equations. The overall framework is illustrated in Figure 2. In this approach, a FET-PINN is used to predict the FET. Considering the prediction error of the model, the predicted temperature is subsequently fused with the temperature calculated by the FET measurement instrument. The implementation steps are as follows:

Step 1 (Calculate the initial predicted temperature): Utilizing the input RDT in conjunction with thermodynamic equations, a FET-PINN model is used to predict the initial FET.

Step 2 (Calculate the fusion weight): The result from step 1 is fused with the temperature computed by the FET measurement instrument, and the fusion weight is determined by nonlinear least squares.

Step 3 (Calculate the final predicted temperature): The fusion weight obtained in step 2 is used in a weighted averaging method to fuse the temperatures and yield the final FET.

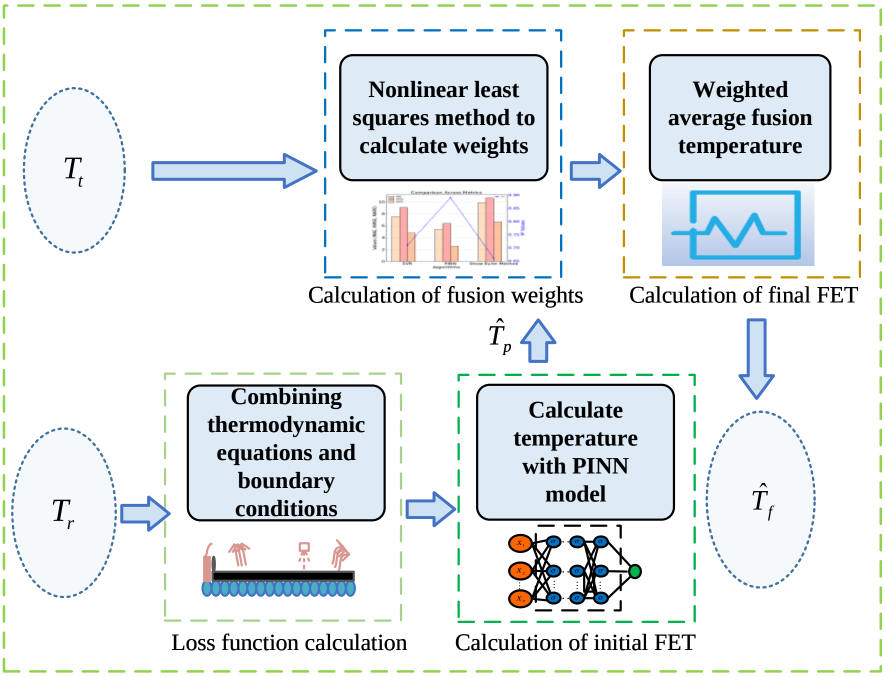

Figure 2. Overall flowchart.

4. FET-PINN prediction of FET based on RDT

4.1. Thermal transfer model in the rolling process

In predicting the FET by incorporating thermodynamic equations, this approach offers significant advantages compared to purely data-driven prediction methods. First, thermodynamic equations can model processes such as heat conduction, convection, and radiation based on physical laws, ensuring that the prediction results better reflect actual physical phenomena. This method reveals the underlying reasons for temperature changes, thereby more accurately reflecting the dynamic variation of the FET. Second, thermodynamic equations effectively incorporate various process parameters and environmental conditions, such as the type of steel and the RDT, which may be neglected or difficult to model accurately in traditional data-driven approaches. By combining these physical factors with thermodynamic principles, the temperature variation in the finishing process can be described more comprehensively, avoiding the overfitting or underfitting issues that might arise from purely data-driven methods. Moreover, thermodynamic equations provide physical constraints to the model, ensuring that the prediction results are physically reasonable [23].

The continuous processing flow from rough rolling to finishing rolling is shown in Figure 1. In this paper, the thermodynamic equations considered include the air-cooling heat transfer model (radiative cooling, contact cooling) and the water-cooling heat transfer model (water-cooling dissipation) [34].

(i) Air-cooling heat transfer model

When the rolled piece is in an air-cooling state, the heat exchange between the rolled piece and the surrounding medium includes radiative cooling, convective cooling with the air, and contact cooling between the rolled piece and the roll gap. Radiative cooling is the primary heat dissipation method for the rolled piece in the air-cooling state, and the effects of other heat transfer modes can be incorporated into the emissivity ε determined based on measured data. Radiative cooling in the air-cooling state can be described by the Stefan-Boltzmann law:

$$dT_1 = \frac{2 \cdot \varepsilon \cdot \sigma}{\rho(T) \cdot C_p(T)} \cdot \left[(T_s + 273)^4 - (T_e + 273)^4\right] \cdot \left(\frac{1}{h} + \frac{1}{w}\right) d\tau_1 \tag{4.1}$$

where ε is the emissivity; σ is the Stefan–Boltzmann constant, in $kg \cdot s^{-3} \cdot K^{-4}$; $\rho(T)$ is the density of the strip steel, in $\mathrm{kg/m^3}$; $C_p(T)$ is the specific heat of the strip steel, in $\mathrm{J/(kg \cdot K)}$; T_s is the temperature of the strip steel, in K; T_e is the ambient temperature, in K; w is the width of the strip steel, in m; $d\tau_1$ is the time duration for which the rolled piece is in the air-cooling state, in s; and h is the thickness of the strip steel, in m.

(ii) Water-cooling heat transfer model

Convection is the main mode of water-cooling heat transfer. The calculation of the temperature drop during water-cooling mainly considers convective heat transfer. The intensity of the convective heat transfer depends not only on the heat transfer characteristics of the object but also primarily on the physical properties and flow characteristics of the fluid medium. Therefore, convective heat transfer is a very complex process. To facilitate analysis and computation, Newtons law of cooling is commonly used to calculate the heat loss of the strip steel during convective heat transfer.

$$dT_2 = \frac{(T_s - T_w) \cdot f_s \cdot P_s \cdot k}{h \cdot C_p(T_s) \cdot \rho(T_s)} \cdot d\tau_2 \tag{4.2}$$

where k is the water-cooling coefficient, in kg/s^3; f_s is the nozzle water flow rate, in m^3/s; P_s is the nozzle water pressure, in Pa; $d\tau_2$ is the time of heat exchange, in s; T_s is the temperature of the rolled piece, in K; and T_w is the temperature of the cooling medium, in K.

The total heat dissipation is the sum of the dissipation from these two models, i.e., $\Delta T = dT_1 + dT_2$. The final FET is given by $\hat{T}_p = T_r - \Delta T$.

4.2. Construction of the FET-PINN network for FET prediction

The FET-PINN model is shown in Figure 3. By leveraging known thermodynamic equations and boundary conditions to train the neural network, the model does not rely on experimental data. The thermodynamic equation residual term in the loss function ensures that the model adheres to physical laws, while the boundary conditions help the network learn an appropriate temperature distribution. During training, the FET-PINN minimizes the loss function by optimizing the residual of the thermodynamic equations, thereby generating predictions that comply with physical constraints. By combining thermodynamic equations with boundary conditions, the FET-PINN can generate meaningful predictions without experimental data [25–27]. In this paper, the FET-PINN takes time $\tau = [\tau_1, \tau_2]$ and the RDT T_r as inputs, and outputs the predicted FET $\hat{T}_p$.

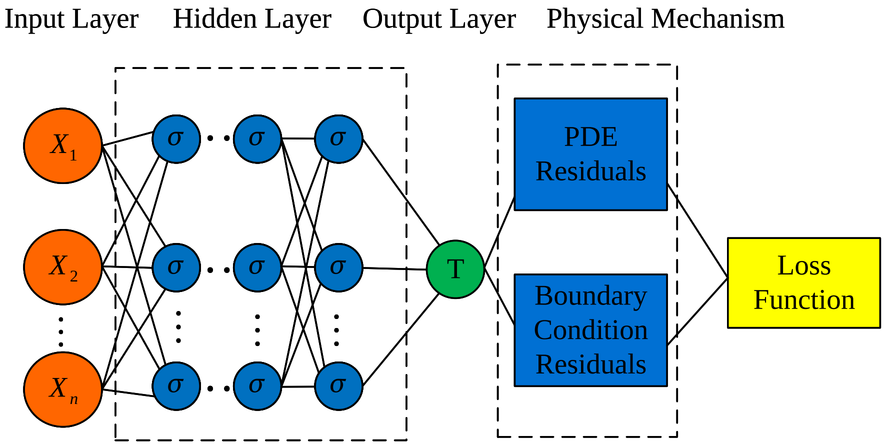

Figure 3. FET-PINN architecture.

The FET-PINN adopts a multilayer perceptron (MLP) architecture comprising an input layer, hidden layers, and an output layer. Its hyperparameters (depth of hidden layers, number of neurons, and activation functions) need to be optimized according to the specific physical problem. For the boundary conditions, at the rough delivery ($\tau = 0$), the strip steel temperature T_r is known. This temperature value provides an initial condition for the model, ensuring that the network prediction at the rough delivery is consistent with the known value, i.e.,

$$\hat{T}_p(\tau = 0) = T_r \tag{4.3}$$

The loss function consists of two main components and is expressed in the form of mean squared error (MSE) as follows:

$$\begin{aligned} \mathcal{L} &= w_t\mathcal{L}_t + w_b\mathcal{L}_b \\ \mathcal{L}_t &= [\hat{T}_p - T_r - \Delta T]^2 \\ \mathcal{L}_b &= \left|\hat{T}_p(\tau = 0) - T_r\right|^2 \end{aligned} \tag{4.4}$$

where $\mathcal{L}$ is the total loss, $\mathcal{L}_t$ is the physical model loss, $\mathcal{L}_b$ is the boundary condition loss, and w_t and w_b are the weighting coefficients.

5. Fusion estimation of the FET

5.1. *Fusion estimation based on predicted and measured temperatures*

The measurement instruments for the FET are limited by various factors such as the measurement location, the surface oxide layer, and thermal radiation. As a result, the actual measured value may not accurately reflect the overall temperature state of the steel. On the other hand, the FET-PINN model predicts the temperature by incorporating physical laws, thereby offering a more theoretical and generalized prediction. However, it relies on input data such as the RDT, and its predictions may exhibit errors under certain operating conditions. Therefore, fusing the predicted temperature with the actual measured temperature can compensate for their respective shortcomings, enhancing the reliability and stability of the prediction results. In this context, the actual measured temperature T_T reduced by the water-cooling temperature drop dT_2 is taken as the measured FET T_t, i.e.,

$$T_t = T_T - dT_2$$

This paper adopts a weighted averaging method to fuse the temperatures:

$$\hat{T}_f = w_p \hat{T}_p + (1 - w_p) T_t \tag{5.1}$$

where $\hat{T}_p$ is the predicted temperature, T_t is the measured FET, and w_p is the weight assigned to the predicted temperature.

5.2. *Optimality of the fusion estimation*

To determine the optimal w_p, this study adopts a nonlinear least squares approach. By comparing the rolling force $\hat{F}_{p,i}$ calculated from the fused temperature $\hat{T}_{f,i}$ with the actual rolling force $F_{f,i}$, the weight w_p is optimized by minimizing the error δ.

According to the SIMS formula, the model of the finishing rolling force is given by [33]

$$F_f = B \cdot l_c^{'} \cdot Q_p \cdot K_m \cdot K_T \tag{5.2}$$

$$K_m = \frac{2}{\sqrt{3}} \sigma_s \tag{5.3}$$

The regression formula for flow stress σ_s is expressed as follows [23, 24]:

$$\sigma_s = \sigma_0 \ \exp\Big(a_1 T + a_2\Big) \left(\frac{u_m}{10}\right)^{\left(a_3 T + a_4\right)} K_s \tag{5.4}$$

$$K_s = a_6 \left(\frac{e}{0.4}\right)^{a_5} - (a_6 - 1) \left(\frac{e}{0.4}\right) \tag{5.5}$$

where F_f is the rolling force, in N; K_m is the average flow stress, in Pa; $l_c^{'}$ is the projected contact length, in m; $B = w$ is the strip width, in m; Q_p is the coefficient accounting for the stress state caused by friction on the arc of contact; K_T is the coefficient accounting for front and back tension effects; σ_s is the flow stress, in Pa; $T = \hat{T}_f$ is the temperature, in K; $u_m = \frac{v_0 h_0}{l_c h_1}$ is the strain rate, in 1/s; V_r is the roll line speed, in m/s; l_c is the contact arc length, in m; h_0, h_1 are the entry and exit thicknesses, in m; $e = \frac{2\Delta h}{3 h_0}$ is the deformation ratio; $a_1 \sim a_6$ are regression coefficients; and σ_0 is the initial flow stress, in Pa.

Thus,

$$f(\hat{T}_{f,i}) = f\Big(w_p \hat{T}_{p,i} + (1 - w_p) T_{t,i}\Big) = B \cdot l_c^{'} \cdot Q_p \cdot K_T \cdot K_m$$

For the i-th sample, define the residual:

$$r_i(w_p) = f\Big(w_p \hat{T}_{p,i} + (1 - w_p) T_{t,i}\Big) - F_{f,i} \tag{5.6}$$

and the mean squared error:

$$\delta(w_p) = \frac{1}{N} \sum_{i=1}^{N} \Big[r_i(w_p)\Big]^2 \tag{5.7}$$

Taking the derivative of $\delta(w_p)$ with respect to w_p and setting it to zero yields the optimality condition:

$$\frac{1}{N}\sum_{i=1}^{N} r_i(w_p)\cdot \left.\frac{df}{d\hat{T}_{f,i}}\right|_{\hat{T}_{f,i}=w_p\hat{T}_{p,i}+(1-w_p)T_{t,i}} \cdot (\hat{T}_{p,i}-T_{t,i}) = 0 \tag{5.8}$$

Let

$$g(w_p) = \frac{1}{N}\sum_{i=1}^{N}\left\{\left[f\Big(w_p\hat{T}_{p,i}+(1-w_p)T_{t,i}\Big)-F_{f,i}\right]\cdot\frac{df}{d\hat{T}_{f,i}}\cdot(\hat{T}_{p,i}-T_{t,i})\right\} = 0$$

Now derive $\frac{df}{d\hat{T}_{f,i}}$. From (5.3), $K_m = \frac{2}{\sqrt{3}}\sigma_s$, so:

$$\frac{df}{d\hat{T}_{f,i}} = B\,l_c'\,Q_p\,K_T\,\frac{2}{\sqrt{3}}\,\frac{d\sigma_s}{d\hat{T}_{f,i}}$$

Let

$$f_1(T_i) = \exp\Big(a_1T_i+a_2\Big), \quad f_2(T_i) = \left(\frac{u_m}{10}\right)^{\left(a_3T_i+a_4\right)}$$

and then

$$\sigma_s = \sigma_0\,K_s\,f_1(T_i)\,f_2(T_i)$$

Note $T_i = \frac{\hat{T}_{f,i}+273}{1000}$, so

$$\frac{dT_i}{d\hat{T}_{f,i}} = \frac{1}{1000}$$

By the chain rule:

$$\frac{d\sigma_s}{d\hat{T}_{f,i}} = \sigma_0\,K_s\,f_1(T_i)\,f_2(T_i)\Big[a_1+a_3\ln\Big(\frac{u_m}{10}\Big)\Big]\frac{1}{1000}$$

and thus,

$$\frac{df}{d\hat{T}_{f,i}} = B\,l_c'\,Q_p\,K_T\,\frac{2}{\sqrt{3}}\cdot\frac{\sigma_0\,K_s}{1000}\,\exp\Big(a_1T+a_2\Big)\left(\frac{u_m}{10}\right)^{\left(a_3T+a_4\right)}\Big[a_1+a_3\ln\Big(\frac{u_m}{10}\Big)\Big] \tag{5.9}$$

Substituting (5.9) into (5.8), and letting

$$T_i = \frac{w_p\hat{T}_{p,i}+(1-w_p)T_{t,i}+273}{1000}$$

we obtain the full expression for the optimality condition:

$$\begin{aligned} g(w_p) = \frac{1}{N}\sum_{i=1}^{N}\Bigg\{&\Big[f\Big(w_p\hat{T}_{p,i}+(1-w_p)T_{t,i}\Big)-F_{f,i}\Big] \\ &\cdot\Bigg[B\,l_c'\,Q_p\,K_T\,\frac{2}{\sqrt{3}}\cdot\frac{\sigma_0\,K_s}{1000}\,\exp\Big(a_1T_i+a_2\Big) \\ &\left(\frac{u_m}{10}\right)^{\left(a_3T_i+a_4\right)}\Big(a_1+a_3\ln\Big(\frac{u_m}{10}\Big)\Big)\Bigg] \\ &\cdot(\hat{T}_{p,i}-T_{t,i})\Bigg\} = 0 \end{aligned} \tag{5.10}$$

Equation (5.10) is a nonlinear equation in w_p. Inspired by the system identification method, the Newton iteration method is finally used to solve for the optimal weight [28–32].

5.3. Solving for the optimal weight w_p via Newton's method

1) Initialization

Set the initial weight w_p^0, convergence tolerance ϵ, finite difference step size Δ, and maximum iterations N_{max}.

2) Compute $g(w_p^{(k)})$

For each sample $i = 1, \ldots, N$, calculate $g(w_p^{(k)})$ based on the current weight:

$$g(w_p^{(k)}) = \frac{1}{N} \sum_{i=1}^{N} r_i \cdot \left.\frac{df}{d\hat{T}_f}\right|_{\hat{T}_{f,i}} \cdot (\hat{T}_{p,i} - T_{t,i}) \tag{5.11}$$

3) Estimate the gradient $g'(w_p^{(k)})$

Since $g'(w_p)$ is complex, we use finite difference approximation:

$$g'(w_p^{(k)}) \approx \frac{g(w_p^{(k)} + \Delta) - g(w_p^{(k)} - \Delta)}{2\Delta} \tag{5.12}$$

4) Update the weight

Use Newton's update formula:

$$w_p^{(k+1)} = w_p^{(k)} - \frac{g(w_p^{(k)})}{g'(w_p^{(k)})} \tag{5.13}$$

5) Convergence check

If $|w_p^{(k+1)} - w_p^{(k)}| < \epsilon$, stop the iteration.

If the iteration count reaches N_{max}, return the current w_p as an approximate solution.

6) Compute the fused temperature

Use Eq (5.1) with optimal w_p^* to compute the fused temperature.

Algorithm 1 presents the Newton iteration process for solving the optimal weight based on the finite difference method. This approach adopts a finite difference method for gradient estimation and applies two stopping criteria: the difference between consecutive iterations is less than ϵ, or the maximum number of iterations is reached. This ensures both accuracy and efficiency.

Algorithm 1: Newton iteration for optimal weight w_p^*

```
Input: Initial weight $w_p^{(0)}$, tolerance $\epsilon$, maximum number of iterations $N_{\max}$, finite difference step
       size $\Delta = 10^{-6}$
Output: Optimal weight $w_p^*$
$k \leftarrow 0$;
repeat;
Compute $g(w_p^{(k)})$ according to Eq (5.11);
Compute the gradient approximation according to Eq (5.12);
Update the weight according to Eq (5.13);
$k \leftarrow k + 1$;
until $|w_p^{(k)} - w_p^{(k-1)}| < \epsilon$ or $k \geq N_{\max}$;
return $w_p^* = w_p^{(k)}$
```

6. Algorithm implementation

Algorithm 2: FET-PINN algorithm for predicting temperature

```
Input: RDT $T_r$, time $\tau$, measured temperature $T_T$
Output: Optimal weight $w_p^*$, fused temperature $\hat{T}_f$
Initialize the neural network $u_{NN}(\tau, T_r, \theta)$;
Initialize parameters $\theta$, weight $w_p^0$, tolerance $\epsilon$, max iterations $N_{\max}$, step size $\Delta$;
while loss function has not converged do
    Compute predicted temperature $\hat{T}_p = u_{NN}(\tau, T_r, \theta)$;
    Compute total loss according to Eq (4.4);
    Update $\theta$ via backpropagation;
Compute error function $g(w_p)$ using Eq (5.11);
Estimate $g'(w_p)$ using finite difference Eq (5.12);
Update $w_p$ using Eq (5.13);
if $|w_p^{(k+1)} - w_p^{(k)}| < \epsilon$ then
    Stop iteration, convergence achieved;
else if $k \geq N_{\max}$ then
    Return current $w_p^{(k+1)}$;
else
    Let $k \leftarrow k + 1$ and continue;
Compute fused temperature from Eq (5.1);
return $w_p^*$, $\hat{T}_f$
```

This paper adopts the FET-PINN to predict the finishing rolling entry temperature. The procedure is shown in Algorithm 2. First, the FET-PINN is constructed with randomly initialized network parameters θ, weight w_p, convergence tolerance ϵ, and maximum number of iterations $N_{\max}$. Then, the loss functions are computed, and gradients are obtained via backpropagation to update the network parameters θ. The model is continuously optimized until the loss function converges, yielding the predicted finishing rolling entry temperature $\hat{T}_p$.

Next, the predicted temperature $\hat{T}_p$ is combined with the actual measured temperature T_t to compute the error function $g(w_p)$ corresponding to the current $w_p^{(k)}$. The derivative $g'(w_p)$ is estimated using finite difference, and $w_p^{(k)}$ is iteratively optimized until convergence. Finally, the optimal weight w_p^* is obtained, and the fused temperature $\hat{T}_f$ is calculated, completing the prediction process.

Remark 6.1. To achieve real-time applicability of the FET-PINN in complex industrial environments, this study introduces an adaptive compression mechanism that maintains high accuracy while reducing latency. The approach integrates model compression, expert-guided configuration, lightweight model management, and online optimization to ensure efficiency and robustness under dynamic conditions. The mechanism is currently under development and undergoing validation.

7. Experimental verification

7.1. Experimental setup

This study focuses on Q235 steel for simulation experiments. The dataset is collected from the hot-rolling production line of Q235 steel at a large steel plant, specifically obtained from the FET measurement system, roughing mill infrared pyrometers, and the pressure sensors of the mill's hydraulic automatic gauge control (AGC) system, recorded during continuous hot-rolling operations. To ensure data quality and suitability for model training, the dataset underwent cleaning and preprocessing, including removing outliers using the 3σ rule, filling missing values through linear interpolation, and applying min-max normalization.

The accuracy and reliability of the predicted entry temperature are then assessed by comparing the actual rolling force F_f with the predicted rolling force $\hat{F}_p$. The coefficient of determination R^2 and RMSE are used to measure the model's overall fitting performance. The MAE is used to evaluate the stability of the errors to avoid the influence of outliers, and MAPE is used to assess the relative deviation of the predicted results from the actual values.

$$R^2 = 1 - \frac{\sum_{i=1}^{n}(y_i - \hat{y}_i)^2}{\sum_{i=1}^{n}(y_i - \bar{y})^2} \tag{7.1}$$

$$RMSE = \sqrt{\frac{1}{n}\sum_{i=1}^{n}(y_i - \hat{y}_i)^2} \tag{7.2}$$

$$MAE = \frac{1}{n}\sum_{i=1}^{n}|y_i - \hat{y}_i| \tag{7.3}$$

$$MAPE = \frac{1}{n}\sum_{i=1}^{n}\left|\frac{y_i - \hat{y}_i}{y_i}\right| \times 100\% \tag{7.4}$$

Here, y_i is the actual value and $\hat{y}_i$ is the predicted value. A larger R^2 indicates better fitting performance; smaller RMSE and MAE indicate smaller average absolute deviation between predicted and actual values; and a smaller MAPE indicates smaller relative percentage error.

Table 1. Hyperparameter configuration of the proposed method (mean ± standard deviation over 5 seeds).

Item	Value
Network structure	2 layers, 50 neurons per layer (searched: 1–6 layers, 50–256 neurons)
Activation function	Tanh (tested ReLU, Swish)
Optimizer	Adam (lr = 1e-3) + L-BFGS fine-tuning
Training time	6.31 ± 0.2 s (Adam: 4.2 s + L-BFGS: 2.1 s)
Error (MAPE)	2.35% ± 0.2%
R^2	0.91 ± 0.003

Table 1 presents the hyperparameter configuration of the proposed method. Through a grid search over the network structure, activation function, and optimization strategy, a 2-layer MLP with 50 neurons per layer and tanh activation is selected. Training is performed using the Adam optimizer (4000 steps) followed by L-BFGS fine-tuning, with a total training time of approximately 6.31 minutes. In terms of stability, repeated experiments over five different random seeds yielded a mean error of 2.35% ± 0.2% and an R^2 above 0.91, indicating that the method is insensitive to initialization and sampling variations.

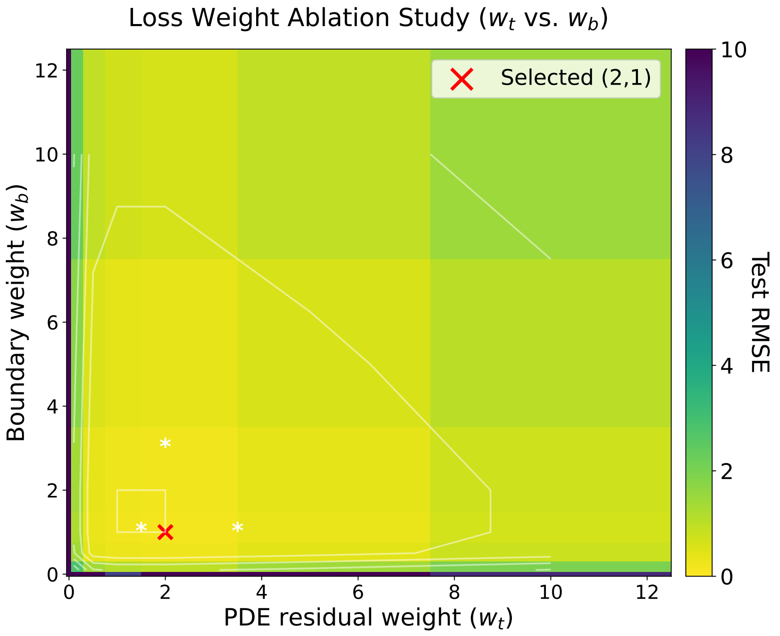

Figure 4. Ablation study of loss function weights.

Figure 4 shows a 2D heatmap of the prediction accuracy (measured by RMSE) under different combinations of the loss function weights w_t (the PDE residual term) and w_b (the boundary condition term). It can be observed that the low-error region forms a distinct "plateau", concentrated in the ranges $w_t \in [1, 5]$ and $w_b \in [0.5, 2]$. The weight configuration used in this study ($w_t = 2$, $w_b = 1$) is located near the center of this low-error plateau and remains within the top 10% optimal region even under sparse observation and noisy conditions.

The initial parameter for the Newton iteration w_p^0 is set to 0.5, with $\epsilon = 10^{-6}$ and $N_{max} = 30$. The proposed regression coefficients are given in [33], and the constant values involved in the proposed equations are listed in Table 2. To comprehensively evaluate the predictive performance of the FET-PINN model, it is compared with support vector regression (SVR) and the explicit Euler method. Cross-validation is also performed on the trained models using Q345 steel. In addition, to assess the appropriateness of the chosen loss weights, a fixed weight of $w_p = 0.5$ is employed for comparison.

Table 2. Descriptions of constants.

Symbol	Physical meaning	Unit	Value
h	Roughing mill exit roll gap (strip thickness)	m	0.02508
σ	Stefan–Boltzmann constant	$\text{kg} \cdot \text{s}^{-3} \cdot \text{K}^{-4}$	$5.67 \cdot 10^{-8}$
ϵ	Thermal emissivity	dimensionless	0.75
k	Water cooling coefficient	kg/s^3	3000
$\rho(T)$	Strip density	kg/m^3	7850
$C_p(T)$	Strip specific heat	$\text{J/(kg} \cdot \text{K)}$	470
T_e	Ambient temperature	K	298.15
w	Strip width	m	2.0
T_w	Cooling medium temperature	K	298.15
f_s	Nozzle water flow rate	m^3/s	$8.33 \cdot 10^{-4}$
P_s	Nozzle water pressure	Pa	$2 \cdot 10^6$
u_m	Deformation speed	1 / s	5
e	Deformation degree	dimensionless	0.778
V_r	Roll line speed	m / s	4
Q_p	Friction influence coefficient	dimensionless	1.1
K_T	Tensile stress influence coefficient	dimensionless	1.05
h_0	Finishing mill entry strip thickness	m	0.02508
h_1	Finishing mill exit strip thickness	m	0.00557
l_c'	Contact horizontal projection length	m	0.0764
l_c	Contact arc length	m	0.077
σ_0	Initial deformation resistance	Pa	$1.506 \cdot 10^8$
a_1	Regression coefficient 1	dimensionless	-2.878
a_2	Regression coefficient 2	dimensionless	3.665
a_3	Regression coefficient 3	dimensionless	0.1861
a_4	Regression coefficient 4	dimensionless	-0.1216
a_5	Regression coefficient 5	dimensionless	0.3795
a_6	Regression coefficient 6	dimensionless	1.402

7.2. Experimental results and analysis

Figure 5 shows the predicted FET corresponding to RDT ranging from 850°C to 1050°C under fixed $\tau_1 = 15$ s and $\tau_2 = 1.5$ s. The corresponding rolling force is then calculated based on the rolling force model, and the four key indicators are evaluated to empirically verify the superiority of the FET-PINN model.

Figure 6 shows a comparison of the rolling force results using the FET-PINN model under optimized and fixed fusion weights. The results indicate that predictions using the optimized weight (blue dots) are closer to the ideal line $y = x$. In contrast, the predictions using the fixed weight $w_p = 0.5$ (orange dots) exhibit larger errors, indicating that nonlinear least squares optimization can more accurately predict rolling force. The final selected fusion weights are $w_p^1 = 0.90$ for FET-PINN, $w_p^2 = 0.88$ for SVR, and $w_p^3 = 0.86$ for the explicit Euler method.

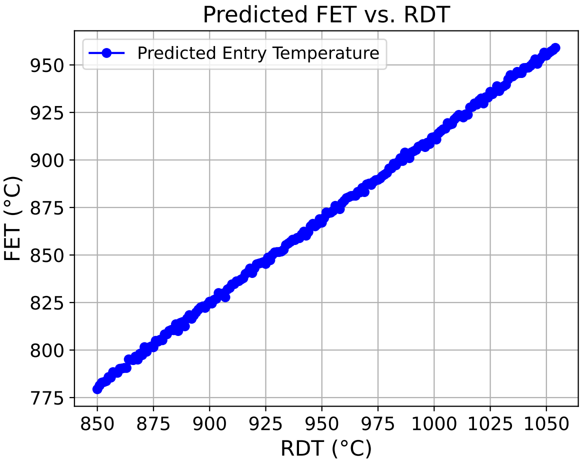

Figure 5. FET variation curve with RDT.

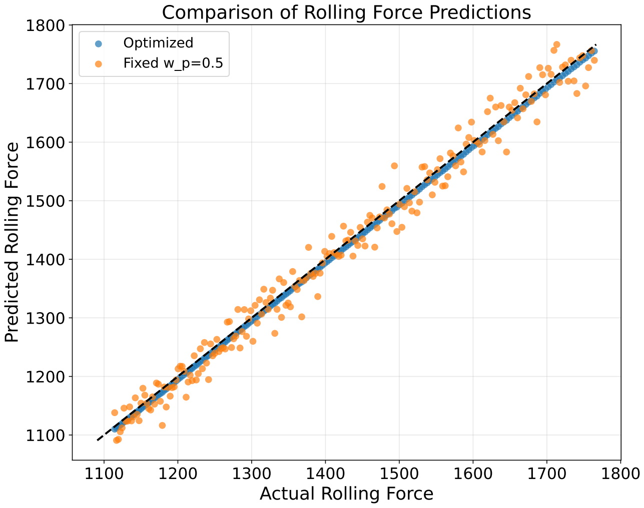

Figure 6. Comparison of optimized and fixed weights.

Table 3. Comparison of algorithm performance indicators.

Algorithm	MAE + σ	RMSE + σ	MAPE + σ	$R^2 + \sigma$
SVR	7.55 ± 0.62	9.06±0.71	4.79% ± 0.35%	0.71 ± 0.005
FET-PINN	5.32 ± 0.41	6.30 ± 0.38	2.35% ± 0.20%	0.91 ± 0.003
Explicit Euler	9.89 ± 0.85	10.69 ± 0.92	6.67% ± 0.58%	0.66 ± 0.007

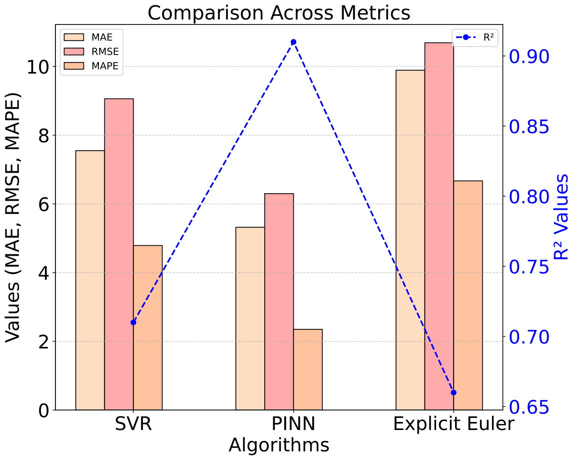

Figure 7. Comparison of various algorithm indicators.

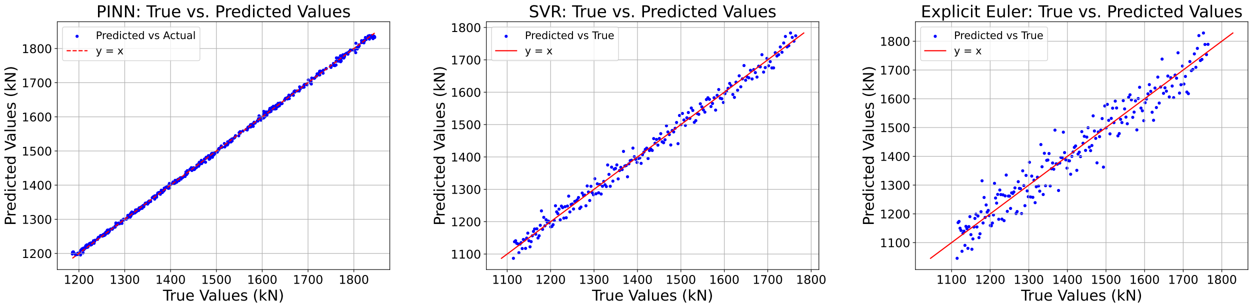

(a) **(b)** **(c)**

Figure 8. (**a**) Scatter plots of predicted vs. actual rolling force for the FET-PINN. (**b**) Scatter plots of predicted vs. actual rolling force for SVR. (**c**) Scatter plots of predicted vs. actual rolling force for the explicit Euler.

As shown in Table 3, and Figures 7 and 8, the predicted rolling forces are very close to the actual ones, and the FET-PINN model outperforms the other two algorithms across all four evaluation metrics. The scatter plots also show that the predictions are concentrated around the line $y = x$, indicating the high accuracy of the predicted entry temperature by the FET-PINN model.

Figure 9 shows the prediction performance of Q345 steel grade under the trained FET-PINN model. The results show that the predicted value is highly consistent with the actual rolling force, verifying the excellent performance of the model in cross-steel grade applications.

7.3. *Comparative experiment*

Table 4 summarizes recent applications of various PINN variants in various fields. These results demonstrate that different PINN variants have been successfully applied to diverse problems, including additive manufacturing [20,22], composite material processing [21], and environmental systems such as river temperature prediction [19]. In contrast, our work targets hot rolling, a representative and complex industrial process where precise temperature prediction is essential for process control.

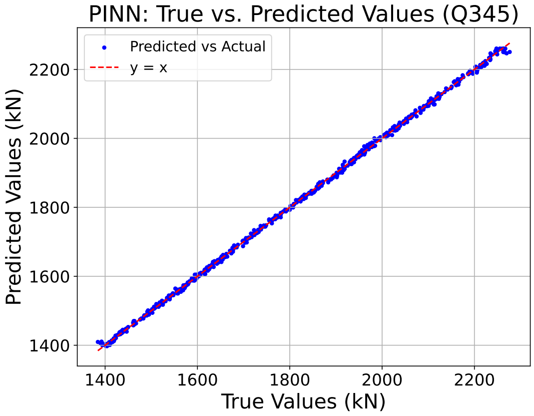

Figure 9. Comparison of predicted and actual rolling forces for Q345 steel.

To further evaluate the generalization and convergence of the proposed FET-PINN, we conducted additional experiments under different training steps (36k, 90k, 125k, and 170k) while keeping the network architecture and hyperparameters fixed. As shown in Figure 10, the FET-PINN consistently achieves lower MAPE than other representative PINN approaches at all training steps, indicating stable convergence and robust performance without oscillation. Notably, most existing studies do not report training or prediction times; only [20] and [21] provided training times of approximately 1.5 hours and 2.5 hours, respectively, with prediction times of 0.001 second. By comparison, the FET-PINN achieves higher prediction accuracy (MAPE = 1.73% at 170k steps) with fewer iterations, highlighting an effective balance between computational efficiency and predictive performance.

Table 4. Comparison of recent PINN-based methods for manufacturing temperature prediction (2023–2025).

Reference	PINN variant	Application scenario	MAPE	Training steps
[19]	PINN-KAN	River temperature prediction	2.3%	36k
[20]	Transfer -learning PINN	Temperature field modeling in additive manufacturing	2.3%	90k
[21]	PINN-LSTM	Composite material temperature prediction	4.8%	125k
[22]	PFNN/FNN	Temperature field prediction in metal additive manufacturing	2.08%	170k
This work	**FET-PINN**	FET prediction in hot rolling	**2.29%**	25**k**

8. Conclusions

In response to the complexity of predicting the FET in hot-rolled strip steel, this paper proposes an innovative hybrid modeling approach that combines the FET-PINN with measured data for collaborative correction. By embedding the thermodynamic evolution of the RDT into the FET-PINN framework, a predictive model with explicit physical constraints is constructed. This effectively balances the low computational efficiency of traditional physical models and the weak interpretability of purely data-

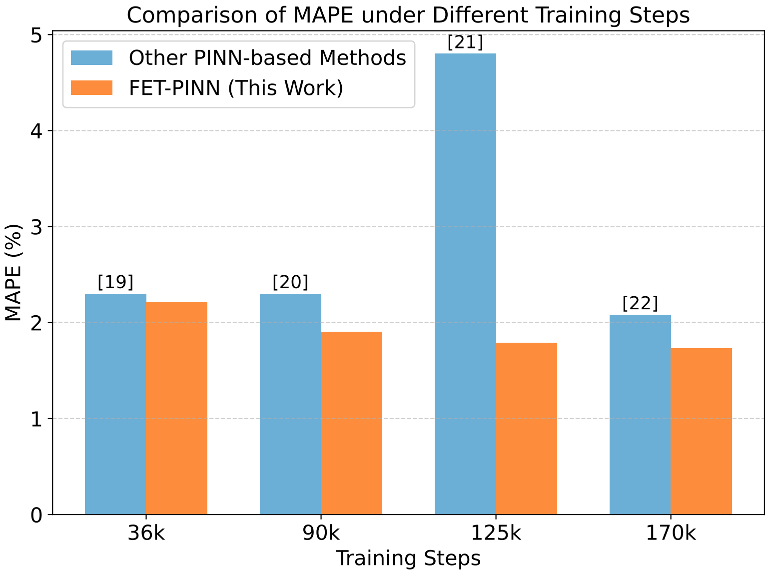

Figure 10. MAPE comparison with reference methods at the same step size.

driven models. Combined with a dynamic calibration mechanism based on real-time measurements from on-site thermometers, the approach significantly improves the engineering applicability of the predicted temperatures and provides a reliable foundation for optimizing rolling process parameters. Compared with conventional numerical and machine learning methods, the proposed method ensures physical consistency while offering fast response capabilities, meeting the requirements of real-time industrial production control. Further analysis demonstrates that enhanced temperature prediction accuracy can improve rolling force settings, reduce energy consumption, and increase dimensional stability of the final product.

The proposed FET-PINN model in this study still has certain limitations, particularly in handling complex multi-physics coupling problems and large-scale geometric computations, where issues such as low training efficiency and numerical instability (e.g., gradient pathologies and loss imbalance) are especially prominent. To address these challenges, future research can focus on the following directions: (i) developing novel FET-PINN variants with improved network architectures to enhance modeling capability for complex physical fields; (ii) improving model generalization under diverse operating conditions by incorporating additional key process parameters and establishing a multi-variable, multi-scale integrated prediction framework; and (iii) introducing online adaptive adjustment mechanisms to enable real-time responses to dynamic production changes, thereby significantly increasing practical value in industrial applications.

Use of AI tools declaration

The authors declare that no Artificial Intelligence (AI) tools were used in the creation of this article. All data were obtained from industrial production systems and were thoroughly anonymized. The data complied with confidentiality agreements established with the relevant enterprise. No sensitive or personal information was involved, and all data handling procedures adhered to ethical standards.

Conflict of interest

The authors declare there is no conflicts of interest.

References

1. J. Li, X. Wang, J. Zhao, Q. Yang, H. Qie, Predicting mechanical properties lower upper bound for cold-rolling strip by machine learning-based artificial intelligence, *ISA Trans.*, **147** (2024), 328–336. https://doi.org/10.1016/j.isatra.2024.01.028
2. Y. Ji, S. Liu, M. Zhou, Z. Zhao, X. Guo, L. Qi, A machine learning and genetic algorithm-based method for predicting width deviation of hot-rolled strip in steel production systems, *Inf. Sci.*, **589** (2022), 360–375. https://doi.org/10.1016/j.ins.2021.12.063
3. S. X. Chen, Y. Li, J. Zou, Temperature control system modeling and simulation of finishing mill, *Appl. Mech. Mater.*, **462** (2014), 519–524. https://doi.org/10.4028/www.scientific.net/AMM.462-463.519
4. H. Bo, Y. Zhang, Z. Fei, Q. Guo, J. Zhang, T. Yildirim, Temperature prediction for finish entry of hot strip mill based on data-driven, in *2020 39th Chinese Control Conference (CCC)*, IEEE, (2020), 2487–2493. https://doi.org/10.23919/CCC50068.2020.9188827
5. C. Li, Z. Xia, H. Meng, J. Sun, The research on finish rolling temperature prediction based on deep belief network, in *2018 3rd International Conference on Mechanical, Control and Computer Engineering (ICMCCE)*, IEEE, (2018), 651–654. https://doi.org/10.1109/ICMCCE.2018.00144
6. G. Han, H. Li, J. Zhang, N. Kong, Y. Liu, X. You, et al., Prediction and analysis of rolling process temperature field for silicon steel in tandem cold rolling, *Int. J. Adv. Manuf. Technol.*, **115** (2021), 1637–1655. https://doi.org/10.1007/s00170-021-06993-9
7. Z. Zhang, B. Wang, S. Yuan, Y. Li, J. Yu, T. Li, et al., Deep learning-based prediction framework of temperature control time for wide-thick slab hot rolling production, *Expert Syst. Appl.*, **227** (2023), 120083. https://doi.org/10.1016/j.eswa.2023.120083
8. S. A. Botnikov, O. S. Khlybov, A. N. Kostychev, Development of the metal temperature prediction model for steel-pouring and tundish ladles used at the casting and rolling complex, *Metallurgist*, **63** (2019), 792–803. https://doi.org/10.1007/s11015-019-00891-y
9. J. A. Barrios, C. Villanueva, A. Cavazos, R. Colás, Fuzzy C-means rule generation for fuzzy entry temperature prediction in a hot strip mill, *J. Iron. Steel Res. Int.*, **23** (2016), 116–123. https://doi.org/10.1016/S1006-706X(16)30022-X
10. G. M. Méndez, I. López-Juárez, M. A. Alcorta García, D. C. Martinez-Peon, P. N. Montes-Dorantes, The enhanced Wagner-Hagras OLS-BP hybrid algorithm for training IT3 NSFLS-1 for temperature prediction in HSM processes, *Mathematics*, **11** (2023), 4933. https://doi.org/10.3390/math11244933
11. J. A. Barrios, M. Torres-Alvarado, A. Cavazos, Neural, fuzzy and grey-box modelling for entry temperature prediction in a hot strip mill, *Expert Syst. Appl.*, **39** (2012), 3374–3384. https://doi.org/10.1016/j.eswa.2011.09.025

12. Y. Sun, Q. Zhang, S. Raffoul, Physics-informed neural network for predicting hot-rolled steel temperatures during heating process, *J. Eng. Res.*, **13** (2025), 1496–1504. https://doi.org/10.1016/j.jer.2024.02.011

13. K. Zhang, Y. Wang, K. Peng, A hierarchical feature-fusion-based method for predicting the coiling temperature in a hot rolling mill process, *Control Eng. Pract.*, **164** (2025), 106517. https://doi.org/10.1016/j.conengprac.2025.106517

14. B. Yang, L. Liu, H. Huang, Y. Wang, D. Li, Q. Yang, et al., A real-time temperature field prediction method for steel rolling heating furnaces based on graph neural networks, *Int. J. Heat Mass Transfer*, **235** (2024), 126220. https://doi.org/10.1016/j.ijheatmasstransfer.2024.126220

15. M. M. Almajid, M. O. Abu-Al-Saud, Prediction of porous media fluid flow using physics informed neural networks, *J. Pet. Sci. Eng.*, **208** (2022), 109205. https://doi.org/10.1016/j.petrol.2021.109205

16. H. Bolandi, G. Sreekumar, X. Li, N. Lajnef, V. N. Boddeti, Physics informed neural network for dynamic stress prediction, *Appl. Intell.*, **53** (2023), 26313–26328. https://doi.org/10.1007/s10489-023-04923-8

17. H. Hu, L. Qi, X. Chao, Physics-informed Neural Networks (PINN) for computational solid mechanics: Numerical frameworks and applications, *Thin-Walled Struct.*, **205** (2024), 112495. https://doi.org/10.1016/j.tws.2024.112495

18. C. Han, J. Zhang, Z. Tu, T. Ma, Pinn-afp: A novel cs curve estimation method for asphalt mixtures fatigue prediction based on physics-informed neural network, *Constr. Build. Mater.*, **415** (2024), 135070. https://doi.org/10.1016/j.conbuildmat.2024.135070

19. M. B. Figueredo, M. de J. Ferreira, R. L. S. Monteiro, A. N. Silva, T. B. Murari, Hybrid PINN-LSTM model for river temperature prediction: A physics-informed deep learning approach, *J. Comput. Commun.*, **13** (2025), 115–134. https://doi.org/10.4236/jcc.2025.136008

20. S. Liao, T. Xue, J. Jeong, S. Webster, K. Ehmann, J. Cao, Hybrid thermal modeling of additive manufacturing processes using physics-informed neural networks for temperature prediction and parameter identification, *Comput. Mech.*, **72** (2023), 499–512. https://doi.org/10.1007/s00466-022-02257-9

21. X. Han, J. Li, L. Yuan, X. Zhang, W. Zhu, Y. Liu, et al., PINN and KAN temperature prediction of carbon Fiber/Epoxy composite materials irradiated by nuclear environment simulated intense heat fluxes, *Ann. Nucl. Energy*, **111454** (2025). https://doi.org/10.1016/j.anucene.2025.111454

22. S. Peng, S. Yang, B. Gao, W. Liu, F. Wang, Z. Tang, Prediction of 3D temperature field through single 2D temperature data based on transfer learning-based PINN model in laser-based directed energy deposition, *J. Manuf. Process.*, **138** (2025), 140–156. https://doi.org/10.1016/j.jmapro.2025.02.015

23. Z. Dong, X. Li, F. Luan, L. Meng, J. Ding, D. Zhang, Fusion of theory and data-driven model in hot plate rolling: A case study of rolling force prediction, *Expert Syst. Appl.*, **245** (2024), 123047. https://doi.org/10.1016/j.eswa.2023.123047

24. S. Shen, D. Guye, X. Ma, S. Yue, N. Armanfard, Multistep networks for roll force prediction in hot strip rolling mill, *Mach. Learn. Appl.*, **7** (2022), 100245. https://doi.org/10.1016/j.mlwa.2021.100245

25. K. Nilpueng, P. Kaseethong, M. Mesgarpour, M. S. Shadloo, S. Wongwises, A novel temperature prediction method without using energy equation based on physics-informed neural network (PINN): A case study on plate-circular/square pin-fin heat sinks, *Eng. Anal. Boundary Elem.*, **145** (2022), 404–417. https://doi.org/10.1016/j.enganabound.2022.09.032
26. J. Hua, Y. Li, C. Liu, P. Wan, X. Liu, Physics-informed neural networks with weighted losses by uncertainty evaluation for accurate and stable prediction of manufacturing systems, *IEEE Trans. Neural Networks Learn. Syst.*, **35** (2023), 11064–11076. https://doi.org/10.1109/TNNLS.2023.3247163
27. J. Soibam, I. Aslanidou, K. Kyprianidis, R. B. Fdhila, Inverse flow prediction using ensemble PINNs and uncertainty quantification, *Int. J. Heat Mass Transfer*, **226** (2024), 125480. https://doi.org/10.1016/j.ijheatmasstransfer.2024.125480
28. C. T. Kelley, Newton's method in mixed precision, *SIAM Rev.*, **64** (2022), 191–211. https://doi.org/10.1137/20M1342902
29. P. Yu, Y. Hu, Y. Wang, R. Jia, J. Guo, Optimal consensus control strategy for multi-agent systems under cyber attacks via a stackelberg game approach, *IEEE Trans. Autom. Sci. Eng.*, **22** (2025), 18875–18888. https://doi.org/10.1109/TASE.2025.3591858
30. J. Guo, X. Wang, W. Xue, Y. Zhao, System identification with binary-valued observations under data tampering attacks, *IEEE Trans. Autom. Control*, **66** (2020), 3825–3832. https://doi.org/10.1109/TAC.2020.3029325
31. J. Guo, Q. Zhang, Y. Zhao, Identification of FIR Systems with binary-valued observations under replay attacks, *Automatica*, **172** (2025), 112001. https://doi.org/10.1016/j.automatica.2024.112001
32. R. Jia, T. Wang, W. Xue, J. Guo, Y. Zhao, Multi-time scale consensus algorithm of multi-agent systems with binary-valued data under tampering attacks, *IEEE Trans. Ind. Inf.*, **2025** (2025). https://doi.org/10.1109/TII.2025.3598451
33. H. Li, *Research on Rolling Process Control System and Models for Hot Strip Finishing Mills*, Ph.D thesis, Northeastern University, 2008.
34. D. Chen, Z. L. Li, Y. J. Li, G. Yuan, Research and application of model and control strategies for hot rolled strip cooling process based on ultra-fast cooling system, *ISIJ Int.*, **60** (2020), 136–142. https://doi.org/10.2355/isijinternational.ISIJINT-2019-104